13062–13074 *Nucleic Acids Research, 2021, Vol. 49, No. 22* *Published online 6 December 2021*
https://doi.org/10.1093/nar/gkab1157

Phosphorylation of ribosomal protein S6 differentially affects mRNA translation based on ORF length

Jonathan Bohlen[1,2,3,4,5,*,†], Mykola Roiuk[1,2,3,5,†] and Aurelio A. Teleman[1,2,3,4,5,*]

[1]German Cancer Research Center (DKFZ), 69120 Heidelberg, Germany, [2]CellNetworks - Cluster of Excellence, Heidelberg University, Heidelberg, Germany, [3]Heidelberg University, 69120 Heidelberg, Germany, [4]Heidelberg Biosciences International Graduate School (HBIGS), Germany and [5]National Center for Tumor Diseases (NCT), partner site

Received May 26, 2021; Revised November 04, 2021; Editorial Decision November 05, 2021; Accepted November 08, 2021

ABSTRACT

Phosphorylation of Ribosomal Protein S6 (RPS6) was the first post-translational modification of the ribosome to be identified and is a commonly-used readout for mTORC1 activity. Although the cellular and organismal functions of RPS6 phosphorylation are known, the molecular consequences of RPS6 phosphorylation on translation are less well understood. Here we use selective ribosome footprinting to analyze the location of ribosomes containing phosphorylated RPS6 on endogenous mRNAs in cells. We find that RPS6 becomes progressively dephosphorylated on ribosomes as they translate an mRNA. As a consequence, average RPS6 phosphorylation is higher on mRNAs with short coding sequences (CDSs) compared to mRNAs with long CDSs. We test whether RPS6 phosphorylation differentially affects mRNA translation based on CDS length by genetic removal of RPS6 phosphorylation. We find that RPS6 phosphorylation promotes translation of mRNAs with short CDSs more strongly than mRNAs with long CDSs. Interestingly, RPS6 phosphorylation does not promote translation of mRNAs with 5′ TOP motifs despite their short CDS lengths, suggesting they are translated via a different mode. In sum this provides a dynamic view of RPS6 phosphorylation on ribosomes as they translate mRNAs and the functional consequence on translation.

INTRODUCTION

A large number of post-transcriptional and post-translational modifications of ribosomal RNA and ribosomal proteins have been discovered (1,2), however the impact of these modifications on ribosomal function is often not understood. While modifications of rRNA are implicated in the biosynthesis, catalytic activity and structural integrity of the ribosome (3,4), modifications of ribosomal proteins, which include phosphorylation (5,6), ubiquitinylation (7,8), NEDDylation (9), methylation (10), UFMylation (11) and acetylation (12), are functionally less well understood. Nonetheless, these ribosomal protein modifications are of interest because they can be inducible (5–7), suggesting they could have regulatory functions.

Inducible phosphorylation of ribosomal protein S6 (RPS6) was discovered in mouse livers after injury (6), representing the first known posttranslational modification of the ribosome (13). RPS6 phosphorylation is catalyzed by S6K upon mTORC1 activation, and by RSK upon ERK activation, making it highly responsive to nutrient availability and growth factor signaling (14). As such, p-RPS6 is widely used as a readout of mTOR pathway activation (1,13,14). The functional role of p-RPS6 has been elucidated in yeast (15) and in mice harboring non-phosphorylatable Rps6 (16). Interestingly, while RPS6 phosphorylation does not have a strong impact on growth in either organism, the mutant mice have impaired glucose homeostasis (16), reduced muscle strength (17) and impaired compensatory renal hyperthrophy (18). On a cellular level, loss of RPS6 phosphorylation leads to a higher protein synthesis rate (16), smaller cell size (17,19) and faster proliferation (16). Although these phenotypic consequences of RPS6 phosphorylation at the organismal and cellular levels are clear, the functional consequences of RPS6 phosphorylation at the molecular level are not known. This has been a longstanding open question in the field (1,13,14). Because of the prominent position of RPS6 phosphorylation on the small ribosomal subunit, one hypothesis is that it affects some aspect of ribosome activity such as translation initiation or elongation.

Selective ribosome footprinting is a method that identifies the location of specific ribosome sub-populations on endogenous mRNAs in human cells (20–22). This method employs immunoprecipitation to isolate ribosomes bound

*To whom correspondence should be addressed. Tel: +33 142 75 46 66; Fax: +33 1 42 75 42 24; Email: Jonathan.bohlen@institutimagine.org
Correspondence may also be addressed to Tel: +49 6221 42 1620; Fax: +49 6221 42 1629; Email: a.teleman@dkfz.de
†The authors wish it to be known that, in their opinion, the first two authors should be regarded as Joint First Authors.

© The Author(s) 2021. Published by Oxford University Press on behalf of Nucleic Acids Research.
This is an Open Access article distributed under the terms of the Creative Commons Attribution-NonCommercial License (http://creativecommons.org/licenses/by-nc/4.0/), which permits non-commercial re-use, distribution, and reproduction in any medium, provided the original work is properly cited. For commercial re-use, please contact journals.permissions@oup.com

to specific factors such as initiation factors or chaperones, followed by sequencing of their footprints to identify their locations. Here, we adapt this method to look at post-translational modifications of the ribosome. By immunoprecipitating ribosomes phosphorylated on RPS6, we study the location and frequency of phospho-RPS6 ribosomes on endogenous mRNAs in human and mouse cells. We find that ribosomes become progressively dephosphorylated on RPS6 as they move along an mRNA to translate the coding sequence (CDS). This dephosphorylation is rather slow compared to ribosome movement, so that it only becomes appreciable on mRNAs with long coding sequences. We find that RPS6 phosphorylation promotes translation most of mRNAs with short CDSs, where it is most abundant. Interestingly, mRNAs containing a 5′ TOP motif defy this general pattern despite being short, and are not sensitive to RPS6 phosphorylation for their efficient translation, leading to a relative increase in ribosomal proteins in RPS6 phospho-deficient cells. This work thereby provides a dynamic view of phosphorylation on RPS6 as ribosomes move along mRNAs, as well as a molecular functional outcome for this post-translational modification.

MATERIALS AND METHODS

Cell culture

HeLa cells and MEF cells were cultured in DMEM + 10% fetal bovine serum + 100 U/ml penicillin/streptomycin (Gibco 15140122). Cells were sub-cultured using trypsin–EDTA for dissociation.

Immunoblotting

Cells were lysed using standard RIPA lysis buffer (150 mM NaCl, 1% NP40, 1% (w/v) sodium deoxycholate, 0.1% SDS, 50 mM Tris pH 8) containing protease inhibitors (Roche mini EDTA-free, 1 tablet in 10 ml) and phosphatase inhibitors (2 mM Sodium Ortho-Vanadate, Roche Phosstop 1 tablet in 10 ml, 0.1 M sodium fluoride, 0.1 M beta-glycerophosphate) and benzonase (50 U/ml), after washing briefly with FBS-free DMEM. Lysates were clarified and protein concentration was determined using a BCA assay. Equal protein amounts were run on SDS-PAGE gels and transferred to a nitrocellulose membrane with 0.2 μm pore size. After Ponceau staining, membranes were incubated in 5% skim milk in PBST (134 mM NaCl, 2,7 mM KCl, 5.4 mM Na_2HPO_4, 1.47 mM KH_2PO_4) for 1 h, briefly rinsed with PBST and then incubated in primary antibody solution (5% BSA PBST or 5% skim milk PBST) overnight at 4°C. Membranes were then washed three times 15 min each in PBST, incubated in secondary antibody solution (1:10 000 in 5% skim milk PBST) for 1 h at room temperature, then washed again three times for 15 min. Finally, chemiluminescence was detected using ECL reagents and the Biorad ChemiDoc Imaging System. No membranes were stripped. Antibodies used in this study are listed in Supplementary Table S1.

Immunoprecipitation

One million HeLa cells or 0.5 million MEF cells were seeded per well of a six-well dish. Cells were treated with 100 nM Torin1 for 30 min. Cells were washed briefly with FBS-free growth medium, then lysed in 200 μl lysis buffer (0.5 M HEPES pH 7.5, 10 mM $MgCl_2$, 0.2 M KCl, 1% NP40, 200 μM CHX, 0.1 M NaF, 0.011 g/ml β-glycerophosphate, 2 mM sodium vanadate, PhosSTOP™ (Roche 04 906 845 001) and cOmplete™ Mini (Roche 11836153001) both at 2× the suppliers indicated concentration, tablet dissolved in water) per well. Cells were scraped off the plate and the collected lysate was transferred to a 1.5 ml reaction tube. Lysates were clarified at 20 000g for 10 min, at 4°C. Input samples were saved by transferring 80 μl of the lysate into a fresh tube, and the rest of the lysate was used for immunoprecipitation: Protein A magnetic beads (Thermo 10001D) were prepared according to the manufacturer's instructions. For the IP from HeLa cell lysates, 100 μl of magnetic beads and 10 μl of anti-p-RPS6 (Ser235/236) (Cell signaling #4857) were used per condition. For the IP from MEFs, 50 μl of magnetic beads and 20 μl of antibody were used per condition. Beads were washed three times and then added to the lysates. Lysates with beads were incubated for 2 h, rotating at 4°C. Then beads were washed three times with bead wash buffer (20 mM Tris pH 7.4, 10 mM $MgCl_2$, 140 mM KCl, 1% NP40), including a change of tube during the last wash. Beads were split into two aliquots. To one of them 1× Laemmli buffer was added an beads were boiled at 95°C for 5 min for western blot analysis. The other half was subjected to RNA extraction using TRIzol reagent (Invitrogen 15596026) according to the manufacturer's instructions. RNA was then analysed on an Agilent Bioanalyzer using the total RNA chip.

Immunofluorescence

MEF cells were seeded at 500 000 cells per well of a six-well plate on microscopy coverslips. Medium was removed and cells were fixed with 4% formaldehyde in PBS for 20 min at room temperature. Samples were then washed three times with PBS, then blocked for 45 min with PBS 0.2% Triton 0.1% BSA. Primary anti-*p*-RPS6 (1:1000, Ser235/236, Cell signaling #4857) antibody was incubated for 2 h in PBS, 0.2% Triton, 0.1% BSA at room temperature. Samples were then washed four times with PBS, 0.2% Triton, 0.1% BSA and incubated for 2 h at room temperature with secondary antibody (anti-rabbit, 1:10 000) in PBS, 0.2% Triton, 0.1% BSA. After washing four times with PBS 0.2% Trition, including DAPI in the third wash, samples were equilibrated in mounting medium for 10 min. Cover slips were then mounted on a slide holder and images were taken using a standard cell culture fluorescence microscope.

Immunoprecipitation—Q-RT-PCR

pS6-selective immunoprecipitation was performed in duplicates from HeLa cell lysates, which were prepared as mentioned above. The immunoprecipitated RNA pellet was resuspended in 12 ul of RNase- DNase-free water. 100 μl of lysate was saved and used for total RNA extraction using RNase Mini spin columns (Qiagen, cat. no. 74106). The integrity of RNA was verified on a Bioanalyzer (Agilent). cDNA was generated by reverse transcription (RT) using oligo-dT+ random hexamer primers and Maxima H minus

reverse transcriptase. 8 ul of IP-ed RNA and 1 ug of total RNA served as an input into the RT reaction. The efficiency of Q-RT-PCR primer pairs was checked using a serial dilution of sample. Quantitative RT-PCR was run on a QuantStudio3 instrument with primaQUANT SYBRGreen low ROX master mix. Levels of RNA in the immunoprecipitated sample were normalized to the corresponding mRNA levels detected in the total RNA input sample. Sequences of oligos used for Q-RT-PCR are provided in Supplementary Table S2.

p-RPS6 selective and total ribosome footprinting

HeLa cells were seeded in ten 10 cm dishes at 1.5 million cells per dish in 10 ml growth medium. MEF cells were seeded in three 15 cm dishes per condition at 3 million cells in 20 ml growth medium. Two days later, cells were harvested for Ribo-seq. Cells were briefly rinsed with ice-cold PBS containing 10 mM $MgCl_2$, 200 μM cycloheximide (CHX). This solution was poured off, removed by gently tapping the dish onto paper towels, and cells were lysed with 200 μl of lysis buffer (0.1 M HEPES pH 7.5, 20 mM $MgCl_2$, 0.4 M KCl, 2% NP40, 400 μM CHX, 0.2 M NaF, 0.022 g/ml β-glycerophosphate, 4 mM sodium vanadate, PhosSTOP™ (Roche 04 906 845 001) and cOmplete™ Mini (Roche 11836153001) both at 2× the suppliers indicated concentration, tablet dissolved in water) per plate. Cells were scraped off and lysate was collected in a 1.5 ml tube. The collected volume was roughly 400 μl per plate. After brief vortexing, lysate was clarified by centrifuging for 10 min at 20 000g at 4°C. Approximate RNA concentration was measured using a Nanodrop system and 100 U of Ambion RNAse 1 was added per 120 μg of measured RNA. To prepare undigested polysome profiles RNAse was omitted. Lysates were incubated with RNAse for 5 minutes on ice. Lysates were then pipetted onto 17.5–50% sucrose gradients,which were produced by freezing and layering 50% (2.5 ml), 41.9% (2.5 ml), 33.8% (2.5 ml), 25.6% (2.5 ml) and 17.5% (1.8 ml) sucrose solutions (10 mM Tris–HCl pH 7.4, 10 mM $MgCl_2$, 140 mM KCl, 200 μM CHX) in Seton Scientific Polyclear Tubes 9/16 × 3–3/4 IN, and centrifuged at 35 000 rpm for 3.5 h in Beckmann SW40 rotor. Gradients were fractionated using a Biocomp Gradient Profiler system and 80S fractions were collected for footprint isolation and immunoprecipitation. 500 μl of 80S fractions were saved for total footprint isolation.

For immunoprecipitation, antibodies were bound to protein A magnetic dynabeads (Thermo 10001D) according to the manufacturer's instructions. For the IP from HeLa cells lysates, 100 μl magnetic beads and 60 μl anti-p-RPS6 (Ser235/236) (Cell signaling #4857) were used. For the preparative IP from MEFs, 180 μl magnetic beads and 100 μl antibody were used. Beads were washed three times and then added to the 80S fractions. Fractions with beads were incubated for 2 h, rotating at 4°C. Then beads were washed three times with bead wash buffer (20 mM Tris pH 7.4, 10 mM $MgCl_2$, 140 mM KCl, 1% NP40), including a change of tube during the last wash. Bead volume was increased to ∼500 μl with bead wash buffer. 10% of the sample volume was saved for western blotting analysis of the IP. Total footprint fractions and IPed fractions were then subjected to RNA extraction: 55 μl (1/9th of volume) of 20% SDS was added, 650 μl acid-phenol chloroform (Ambion) was added and the mixture was incubated at 65°C with 1300 rpm shaking for 45 min. Tubes were then placed on ice for 5 min, spun for 5 min at 20 000g and the supernatant was washed once with acid-phenol chloroform and twice with chloroform. RNA was then precipitated with isopropanol, analyzed on an Agilent Bioanalyzer system to asses RNA integrity, and subjected to library preparation (see below). For RNA-seq in MEF cells, 3 million cells were seeded in 15 cm dishes in 20 ml growth medium and harvested two days later using TRIzol according to the manufacturer instructions.

Deep-sequencing library preparation

For 80S footprinting and RNA-seq, libraries were prepared as follows:

Samples were depleted of ribosomal RNA using the Illumina Ribo-Zero Gold kit. Poly-A mRNA was purified from total RNA using the NEB polyA Spin mRNA Isolation Kit. Poly-A mRNA was then fragmented using chemical cleavage in 50 mM NaHCO3 at pH 10, 95°C for 12 min. Then total RNA was processed in parallel with the depleted RNA from 80S ribosome fractions. For size selection, RNA was run on 15% urea–polyacrylamide gels and fragments from 25–35 nt were excised using reference ssRNA of 25 and 35 nucleotides run on a neighboring lane. RNA was extracted from the gel pieces and phosphorylated using T4 PNK. Deep sequencing libraries were prepared from these RNA fragments using the Bio-Scientific NEXTflex Small RNA-Seq Kit v3. DNA was amplified with 11 PCR cycles for the HeLa Ribo-seq samples and 9–14 cycles for the MEF samples. Deep-sequencing libraries were sequenced on the Illumina Next-Seq 550 system.

Data analysis and statistics

Analysis of ribosome footprinting NGS data: Adapter sequences and randomized nucleotides were trimmed from raw reads using cutadapt (https://doi.org/10.14806/ej.17.1.200) with the following commands:

cutadapt –nextseq-trim = 10 –discard-untrimmed -m16 -M45 -O6 -a TGGAATTCTCGGGTGCCAAGG -o '$OUTPUT' '$INPUT' 1>'$REPORT'

cutadapt -u 4 -o '$OUTPU' '$INPUT'

cutadapt -u -4 -o '$OUTPUTFILE' '$INPUT'

Ribosomal RNA and tRNA reads were removed by alignment to human tRNA and rRNA sequences using bowtie2 (35) using the following commands:

bowtie2 -t -p1 -x rRNA -q '$INPUT' –un '$OUTPUT' -S '$TRASH' 2>'$REPORT'

bowtie2 -t -p1 -x tRNA -q '$INPUT' –un '$OUTPUT' -S '$TRASH' 2>'$REPORT'

Then, the remaining reads were separately aligned to the human transcriptome (Ensembl transcript assembly 94) and human genome (hg38) using BBmap (sourceforge.net/projects/bbmap/) with the following command:

bbmap.sh ambiguous = all maxindel = 200000 in = '$FILENAME' out = '$SAMFILE' -Xmx24g bamscript = bs.sh; sh bs.sh

In the human datasets, 13001 genes had transcripts that passed the depth threshold of 64 raw reads per transcript in all sequencing libraries. In the mouse dataset, 10141 genes passed this threshold. Number and percentage of sequencing reads retained after each major processing step for each deep-sequencing library contained in this study are supplied in Supplementary Table S3. Read counting (Figures 1E–I, 2C–D, 3A–B, C–D, 3F–G, 4A, C, 5A–D S1A, S2A, S3E, S3G–H, S4A–C), metagene plots (Figures 1C–D, 2B, 4D, 3E, S3C–D, S4D), single transcript traces (Figures 2A, 4B and S2B), metagene plots with position buckets (Figures 2C, 4E, S3F), as well as removal of transcripts with PCR artefacts were done with custom software written in C available on GitHub (https://github.com/aurelioteleman/Teleman-Lab). Generally, read counts were normalized to sequencing depth (number of alignments per library). Normalized read counts per coding sequence and basic transcript annotation information is supplied in Supplementary Table S4 for the human data and Supplementary Table S5 for the mouse data. Translation efficiency (TE) was calculated as the normalized number of 80S ribosome footprints in a coding sequence divided by the normalized number of RNA sequencing reads in the coding sequence. For PANTHER Gene Set Enrichment test (Figure 4A), a list of all detected genes (raw reads > 63) and their change in translation between control wildtype and rps6$^{p-/-}$ cells was entered into the panther suite (25) and enrichment for gene sets of cellular components was calculated.

Bioinformatic classification of ER-translated versus cytosolic mRNAs (Figure 3C) was taken from (26), as described in their Supporting Materials and Methods: 'Similar to the yeast secretome, we defined the mammalian secretome as the set of proteins predicted to have a signal peptide or transmembrane domain but excluding known mitochondrial proteins. The set of proteins predicted to contain a signal peptide or transmembrane domain by Phobius were filtered to remove proteins annotated in MitoCarta (53) or associated with the gene ontology term GO:005739 (cellular component 'mitochondrion') to yield the mammalian secretome.' Classification of mRNAs experimentally determined to be translated on the ER (Figure 3D and E) was also taken from (26): In their Supplementary Table S6, column S ($\log_2$(enrichment pulldown versus input)) was used and a threshold of >0.5 was set to classify the detected mRNAs ($n = 4023$) into ER bound ($n = 620$) or unbound ($n = 3403$).

As a non-parametric method to test whether two samples originate from the same distribution we used a Mann–Whitney test. For multiple sample comparison (i.e. >2 samples), the Kruskal–Wallis test was used, which is an extension of the Mann–Whitney test for multiple groups.

Data and software availability

All deep sequencing datasets have been submitted to NCBI Geo (GSE168977). Custom software is available on GitHub: https://github.com/aurelioteleman/Teleman-Lab.

RESULTS

Ribosomes with phospho-S6 are depleted from mRNAs with long ORFs

We aimed to use selective ribosome footprinting (20,22,23) to determine the position on endogenous mRNAs of ribosomes containing phosphorylated Ribosomal Protein S6 (RPS6) (Figure 1A). For this purpose, specific immunoprecipitation (IP) of phosphorylated ribosomes is necessary, hence we assessed the specificity of a monoclonal antibody that recognizes RPS6 when phosphorylated on Serine 235 and 236 (Figure 1B): We used Torin1 treatment as a negative control for the IP, since it inhibits mTOR and as a consequence S6K, leading to a strong reduction in RPS6 phosphorylation in HeLa cells (Input, Figure 1B). Immunoprecipitation of p-RPS6 in control conditions led to co-immunoprecipitation of ribosomal proteins such as RPS15 and of ribosomal RNA (IP, Figure 1B and Supplementary Figure S1A), indicating that the p-RPS6 IP is pulling down entire ribosomes. Treatment with Torin led to a strong reduction in immunoprecipitated p-RPS6 and co-immunoprecipitated RPS15 (IP, Figure 1B). The amount of RNA in the p-RPS6 IP dropped by >80% upon Torin treatment (Figure 1B). From this, we conclude that in the control condition more than 80% of the precipitated RNA is specific for RPS6 phosphorylation, and therefore our p-RPS6 IP is suitable for our purpose. For selective ribosome footprinting, we used ∼7 μg of RNA co-precipitated with pRPS6 antibody from RNAse treated, purified 80S ribosomes. We then generated footprint libraries from the p-RPS6 immunoprecipitation ('pS6-ribosomes') and from total ribosomes and sequenced them. Footprints from both pS6-ribosomes and total ribosomes displayed the expected triplet periodicity, enrichment in Open-Reading Frames (ORFs), and footprint length distribution of translating 80S ribosomes (Figure 1C, D and Supplementary Figure S1B). Generally, pS6-ribosomes have a similar distribution to total ribosomes both within transcripts (Figure 1C, D) and between different mRNAs in the transcriptome (Figure 1E). Nonetheless, pS6-ribosomes were not equally bound to all mRNAs in the transcriptome. For every individual transcript we calculated the relative proportion of bound ribosomes that are phosphorylated on RPS6 by dividing the number of pS6-ribosome footprints to the number of total ribosome footprints ('pS6 abundance'). A z-vs-z analysis revealed that mRNAs from 1637 genes had lower pS6 abundance than expected by chance, and 69 genes had higher pS6 abundance than expected (Figure 1F, and red/blue colored dots in Figure 1E). We reasoned that some property of these 1637 transcripts might cause them to have reduced pS6 abundance. We analyzed various features and found that the transcripts with low pS6 abundance were significantly enriched for long coding sequences (Figure 1G), but not long 5′UTRs or 3′UTRs (Figure 1H-I).

RPS6 phosphorylation is progressively removed from translating ribosomes, particularly on long open-reading frames

We sought to understand why RPS6 phosphorylation is less present on ribosomes translating long ORFs compared to short ORFs. We noticed that on long ORFs, pS6 footprints

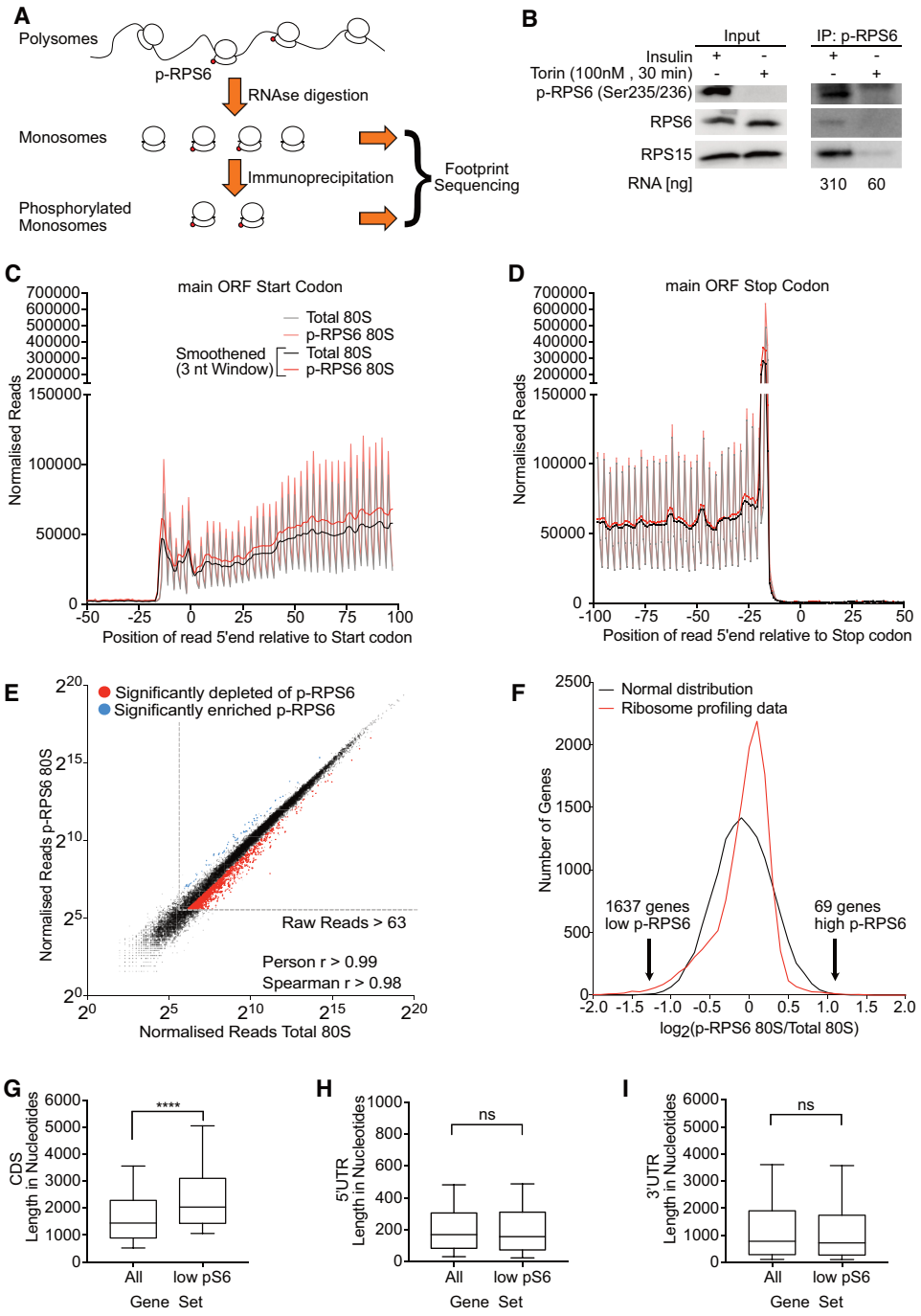

Figure 1. Modification-selective ribosome footprinting reveals the distribution of ribosomes containing phosphorylated RPS6 on mRNAs in vivo. (**A**) Schematic diagram illustrating phospho-RPS6-selective ribosome footprinting. Polysomes are digested by RNAse 1, monosomes are isolated by sucrose density centrifugation, ribosomes containing phosphorylated RPS6 are purified by immunoprecipitation, and footprints are then extracted and sequenced. (**B**) Verification of specificity of the p-RPS6 immunoprecipitation. Ribosomes phosphorylated on RPS6 Serine 235 and 236 were immunoprecipitated from whole cell lysates of control cells or cells treated with Torin (100 nM, 30 min). Low levels of RNA and RPS15 (<20% of control) were obtained in the IP from Torin-treated cells. (**C**, **D**) Metagene profiles for total and p-RPS6 selective 80S ribosome footprints from HeLa cells showing the position of the 5′end of ribosome footprints relative to (C) start and (D) stop codons of all transcripts. Read counts were normalized to sequencing depth. 'Smoothened' indicates the curve was smoothened with a 3nt sliding window. (**E**) Generally, p-RPS6 ribosomes are present on all mRNAs, as can be seen from the tight correlation between pRPS6-ribosome footprints and total 80S footprints. Nonetheless, some transcripts have lower (red) or higher (blue) p-RPS6 ribosome occupancy than expected (determined by z-vs-z analysis in panel F). Reads counts per gene are normalized to library sequencing depth. A minimum threshold of >63 raw reads was set. (**F**) Identification of transcripts with low or high p-RPS6 ribosome occupancy by z-vs-z analysis. Histogram of relative p-RPS6 ribosome occupancy per transcript (red) versus a normal distribution with the same mean, standard deviation, and area under the curve (black). 1637 genes with low p-RPS6 ribosome occupancy and 69 genes with high p-RPS6 occupancy were identified by z-vs-z analysis. (**G–I**) Transcripts with low p-RPS6 occupancy ($n = 1637$) have long coding sequences (G) but not long 5′UTRs (H) or 3′UTRs (I). Line = median, boxes = upper and lower quartile boundaries, whiskers = first and last decile boundaries. *P*-values were determined using unpaired, two-sided Mann–Whitney tests, ****$P < 0.0001$

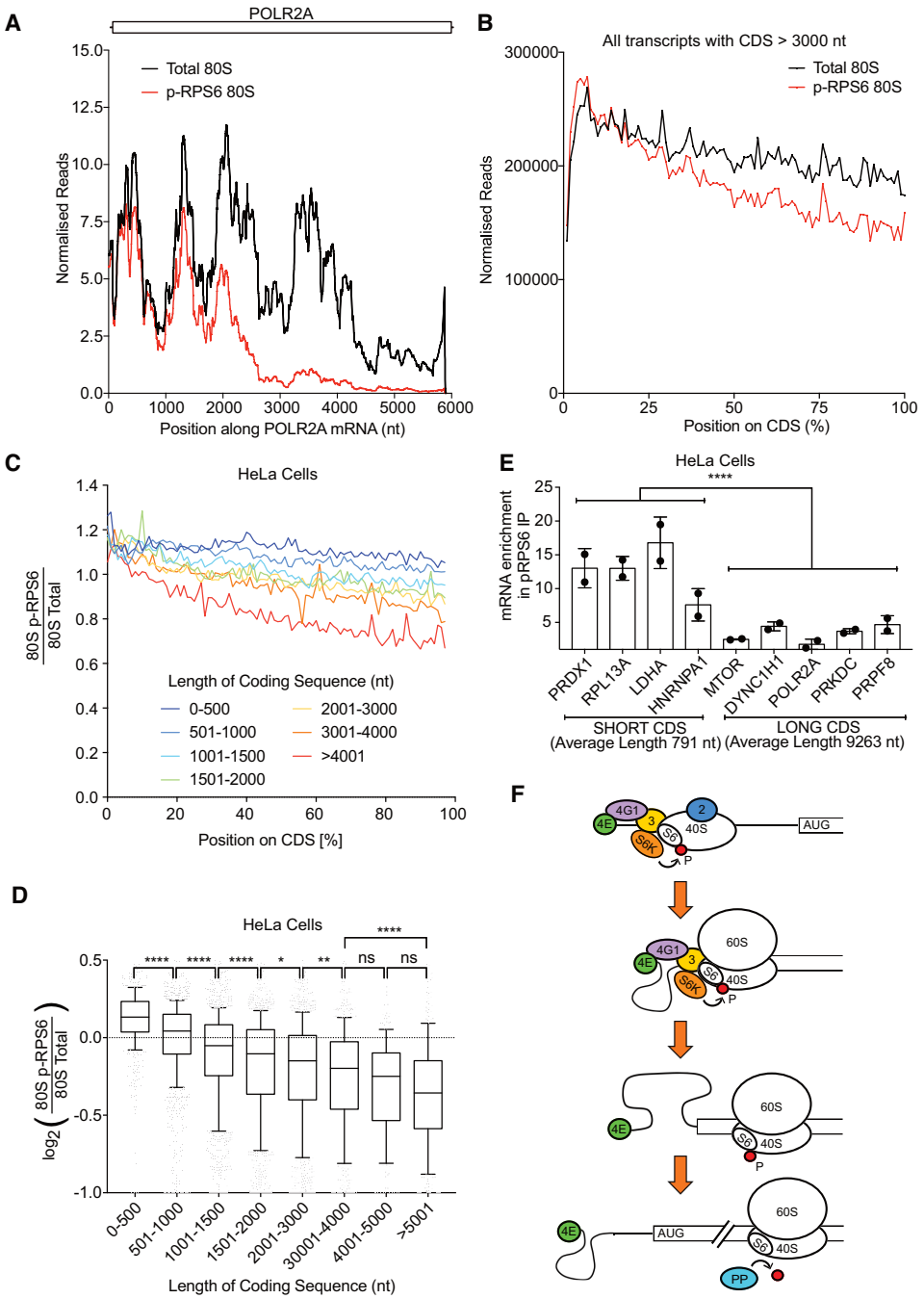

Figure 2. Ribosomes translating long coding sequences are progressively dephosphorylated on RPS6. (**A**) Ribosomes translating the POLR2A mRNA are progressively dephosphorylated on RPS6 Serine 235 and 236. Ribosome occupancy of total 80S and p-RPS6 80S ribosomes along the POLR2A mRNA. Curves are normalized to sequencing depth and smoothened with a sliding window of 200 nucleotides. (**B**) Progressive loss of RPS6 phosphorylation on ribosomes translating long coding sequences can be observed transcriptome-wide. Metagene plot of total 80S and p-RPS6 80S footprints on CDSs longer than 3000nt ($n = 4573$). Position along CDS is scaled from 0% (start codon) to 100% (stop codon). Curves are normalized to sequencing depth. (**C**) Progressive RPS6 dephosphorylation is more pronounced on long CDS mRNAs. Grouped analysis of pRPS6 80S ribosome occupancy normalized to total 80S ribosome occupancy along mRNA groups of different lengths. Positions on mRNAs of different length are all scaled to relative positions between 0% and 100%. (**D**) Coding sequence length inversely correlates with average p-RPS6 occupancy on transcripts. Grouped analysis of the relationship between coding sequence length and p-RPS6 occupancy in HeLa cells. Transcripts were classified into the indicated groups depending on their annotated coding sequence length. Line = median, boxes = upper and lower quartile boundaries, whiskers = first and last decile boundaries. *P*-values were determined using unpaired, two-sided Kruksal Wallis tests, *P*-values were adjusted for multiple testing using statistical hypothesis testing, $*P < 0.0332$, $**P < 0.0021$, $****P < 0.0001$ **(E)** Short CDS mRNAs are more frequently associated with pRPS6 than long CDS mRNAs. Association of mRNAs with pRPS6 ribosomes as determined by pRPS6 immunoprecipitation from crosslinked whol-cell lysates followed by RNA extraction and qRT-PCR. Enrichment in IP (levels in IP / levels in whole cell lysate) is shown. Mann–Whitney test was used to calculate the statistical significant of different outcomes between long and short CDS mRNAs. $****P < 0.0001$. Results from two biological replicates are shown. (**F**) Schematic model of RPS6 phosphorylation by S6K during translation initiation and subsequent dephosphorylation during translation elongation.

A Gene set enrichment, sorted by $\log_2\left(\frac{\text{80S p-RPS6}}{\text{80S Total}}\right)$

PANTHER Enrichment Test: Cellular Component	over-representation	p-value with FDR correction
plasma membrane part	low pRPS6	<0.00000001
nucleus	high pRPS6	<0.00000001
intracellular organelle part	high pRPS6	<0.00000001
cytosolic part	high pRPS6	<0.00000001

B Gene set overrepresentation among 1637 genes with low p-RPS6 occupancy:

PANTHER GO Enrichment: Cellular Component	Fold-Enrichment	p-value with FDR correction
integral component of plasma membrane	2.7	3.03E-19
plasma membrane part	2.2	1.70E-22
plasma membrane protein complex	2.03	1.81E-03
cytoplasm	0.61	5.61E-18
cytosol	0.46	9.17E-06
nucleoplasm part	0.39	9.68E-04
nuclear chromosome	0.39	1.41E-02
nuclear lumen	0.37	5.09E-09
nucleolus	0.15	1.23E-04

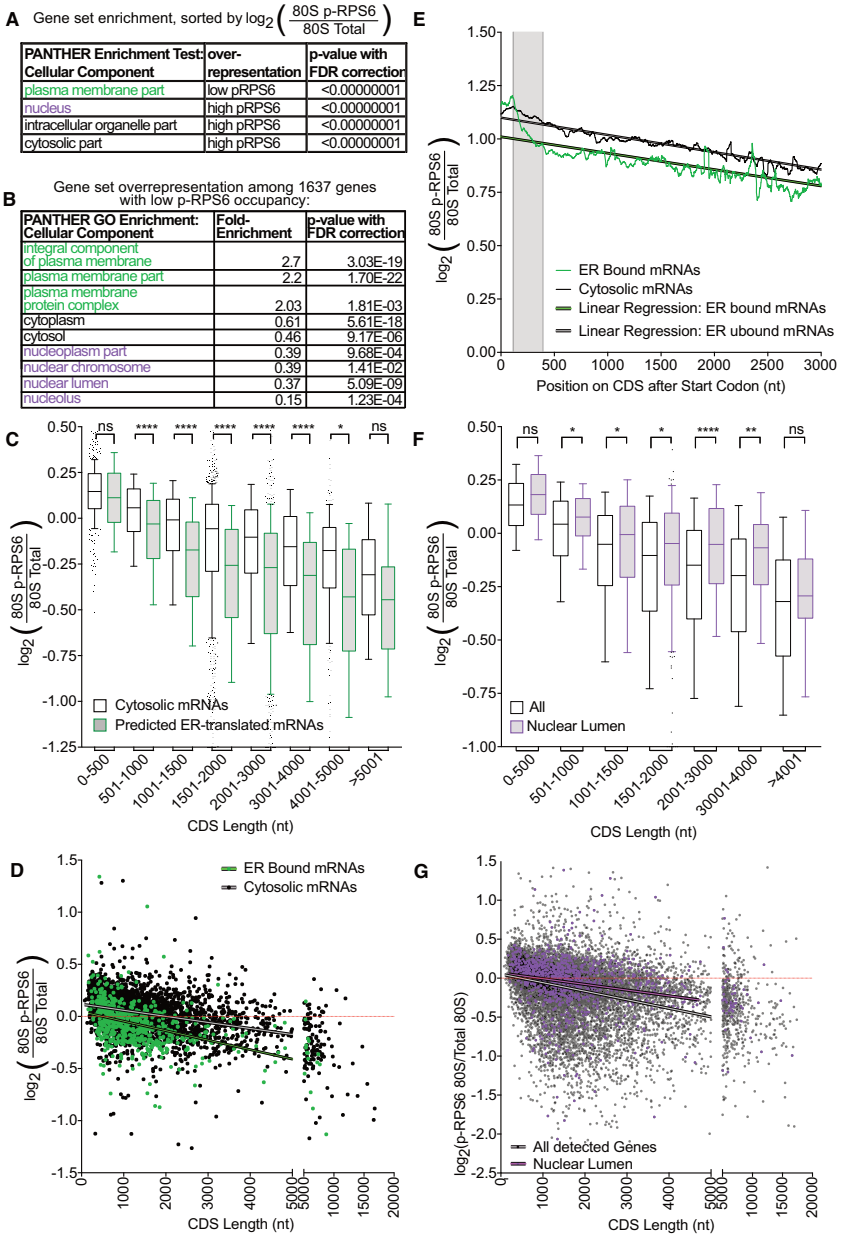

Figure 3. Dephosphorylation of ribosomes on RPS6 is dependent on the subcellular localization of mRNA translation. (A, B) Ribosomes translating mRNAs encoding plasma membrane proteins are enriched for low pRPS6 abundance while ribosomes translating mRNAs encoding nuclear components are enriched for high p-S6 abundance. (**A**) For each transcript the ratio of p-RPS6 / Total ribosome footprints was calculated and GO Enrichment analysis for cellular component was then computed using PANTHER. Representative, significantly enriched or depleted GO terms are shown here; The full list is provided as Supplementary Table S2. (**B**) Over or underrepresentation of cellular component GO terms in the 1637 genes with significantly low p-RPS6 occupancy was determined using PANTHER overrepresentation analysis. Representative, significantly enriched or depleted GO terms are shown here; The full list is provided as Supplementary Table S3. (C–E) Ribosomes translating secreted proteins are more strongly dephosphorylated on RPS6. (**C**) Grouped analysis of the relationship between coding sequence length and p-RPS6 occupancy for mRNAs predicted to be translated on the ER versus all other mRNAs. Transcripts were classified into the indicated groups depending on their annotated coding sequence length and whether they were classified as ER-associated in (26) (see Materials and Methods). Line = median, boxes = upper and lower quartile boundaries, whiskers = first and last decile boundaries. *P*-values were determined using unpaired, two-sided Kruksal Wallis tests, *P*-values were adjusted for multiple testing using statistical hypothesis testing, $*P < 0.0332$, $****P < 0.0001$. (**D**) Scatter plot of $\log_2$(p-RPS6 Enrichment) versus coding sequence length for mRNAs experimentally validated in (26) to be ER-translated (green) or cytosolically translated (black). Linear regression of each group is also shown. (**E**) Metagene plot of the ratio of p-RPS6 80S to total 80S footprints on CDSs for mRNAs as in panel D. Curves are normalized to sequencing depth and smoothened with a sliding window of 40 nucleotides. Linear regression of each curve is also shown. (**F**, **G**) Ribosomes translating nuclear genes are more resistant to dephosphorylation on RPS6. (F) Grouped analysis of the relationship between coding sequence length and p-RPS6 occupancy for mRNAs encoding nuclear lumen proteins (GO:0031981) versus all detected genes. Transcripts were classified into the indicated groups depending on their annotated coding sequence length. Line = median, boxes = upper and lower quartile boundaries, whiskers = first and last decile boundaries. *P*-values were determined using unpaired, two-sided Mann–Whitney tests, *P*-values were adjusted for multiple testing using statistical hypothesis testing, $*P < 0.05$, $**P < 0.005$, $****P < 0.00005$. (G) Scatter plot of $\log_2$(p-RPS6 enrichment) versus coding sequence length for mRNAs encoding nuclear lumen proteins versus all other mRNAs. Linear regression of each group is also shown.

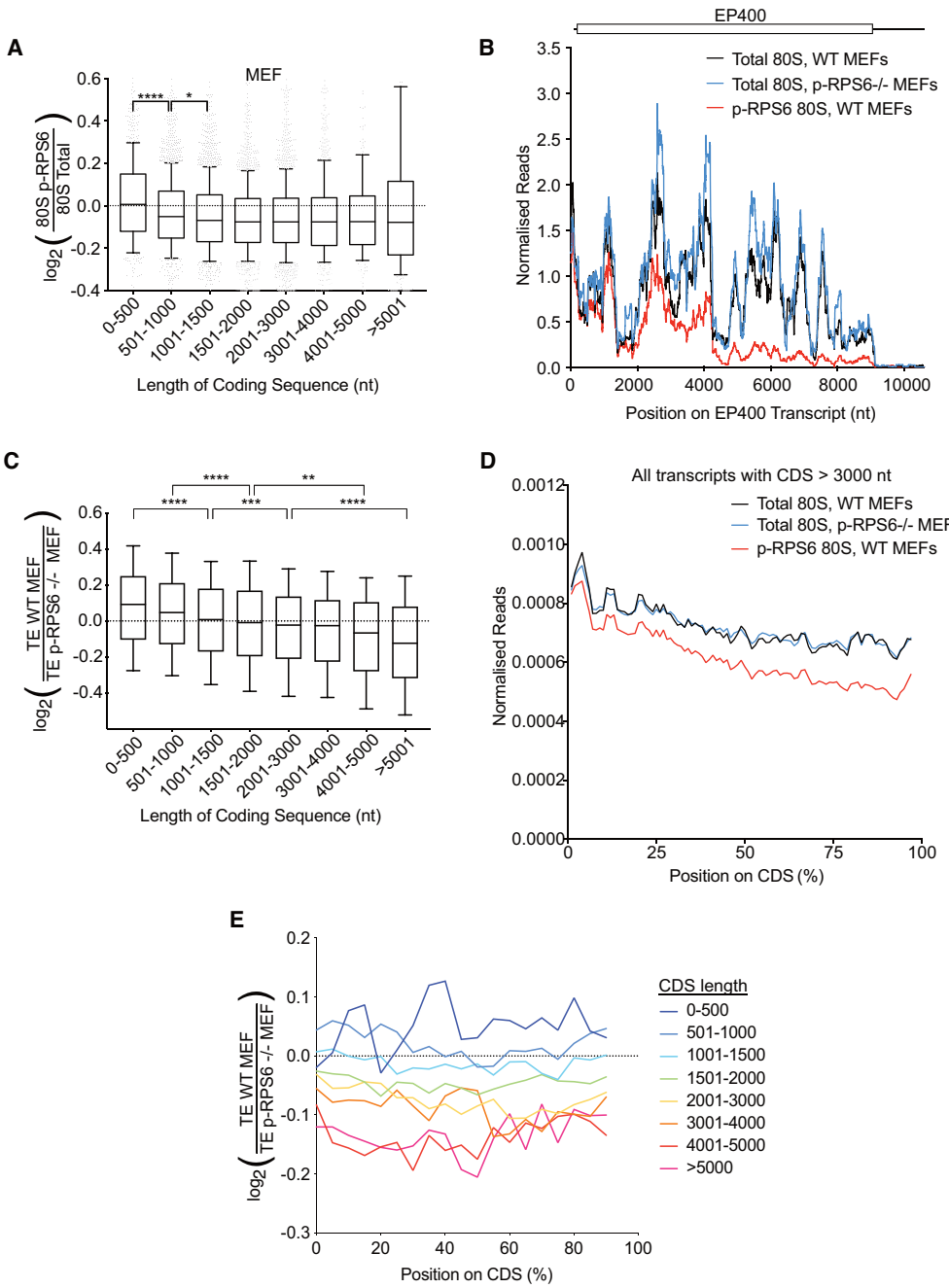

Figure 4. Phosphorylation of RPS6 promotes translation of transcripts with short CDSs. (**A**) As in human cells, average occupancy of phospho-RPS6 ribosomes significantly drops in transcripts with longer CDSs, although the effect is not as large as in HeLa cells. Grouped analysis of the relationship between coding sequence length and p-RPS6 occupancy in mouse embryonic fibroblasts. Transcripts were classified into the indicated groups depending on their annotated coding sequence length. Line = median, boxes = upper and lower quartile boundaries, whiskers = first and last decile boundaries. *P*-values were determined using unpaired, two-sided Kruksal Wallis tests, *P*-values were adjusted for multiple testing using statistical hypothesis testing, $*P < 0.0332$, $****P < 0.0001$. (**B**) Ribosomes translating the EP400 mRNA are progressively dephosphorylated on RPS6 Serine 235 and 236. Ribosome occupancy of total 80S and p-RPS6 80S ribosomes along the EP400 mRNA. Curves are normalized to sequencing depth and smoothened with a sliding window of 200 nucleotides. (**C**) pRPS6 promotes translation of short transcripts. Grouped analysis of the relationship between coding sequence length and relative translational efficiency in control MEFs compared to $rpS6^{P-/-}$ MEFs. Genes were classified into the indicated groups depending on their annotated coding sequence length. Line = median, boxes = upper and lower quartile boundaries, whiskers = first and last decile boundaries. *P*-values were determined using unpaired, two-sided Kruksal–Wallis tests, *P*-values were adjusted for multiple testing using statistical hypothesis testing, $**P < 0.0021$, $***P < 0.0002$, $****P < 0.0001$. (**D**) Progressive dephosphorylation of RPS6 on ribosomes translating long coding sequences in MEFs. Metagene plot of footprints on CDSs longer than 3000nt ($n = 5342$). Position along CDS is scaled from 0% (start codon) to 100% (stop codon). Curves normalized to sequencing depth. (**E**) Ribosome occupancy is uniformly affected across the entire length of the CDS depending on CDS length in control versus $rpS6^{P-/-}$ MEFs. Transcripts were classified into the indicated groups depending on their annotated coding sequence length. Curves denote the ratio in ribosome occupancy between control MEFs and $rpS6^{P-/-}$ MEFs at various positions along the coding sequence, scaled from 0% (start codon) to 100% (stop codon). Curves normalized to sequencing depth.

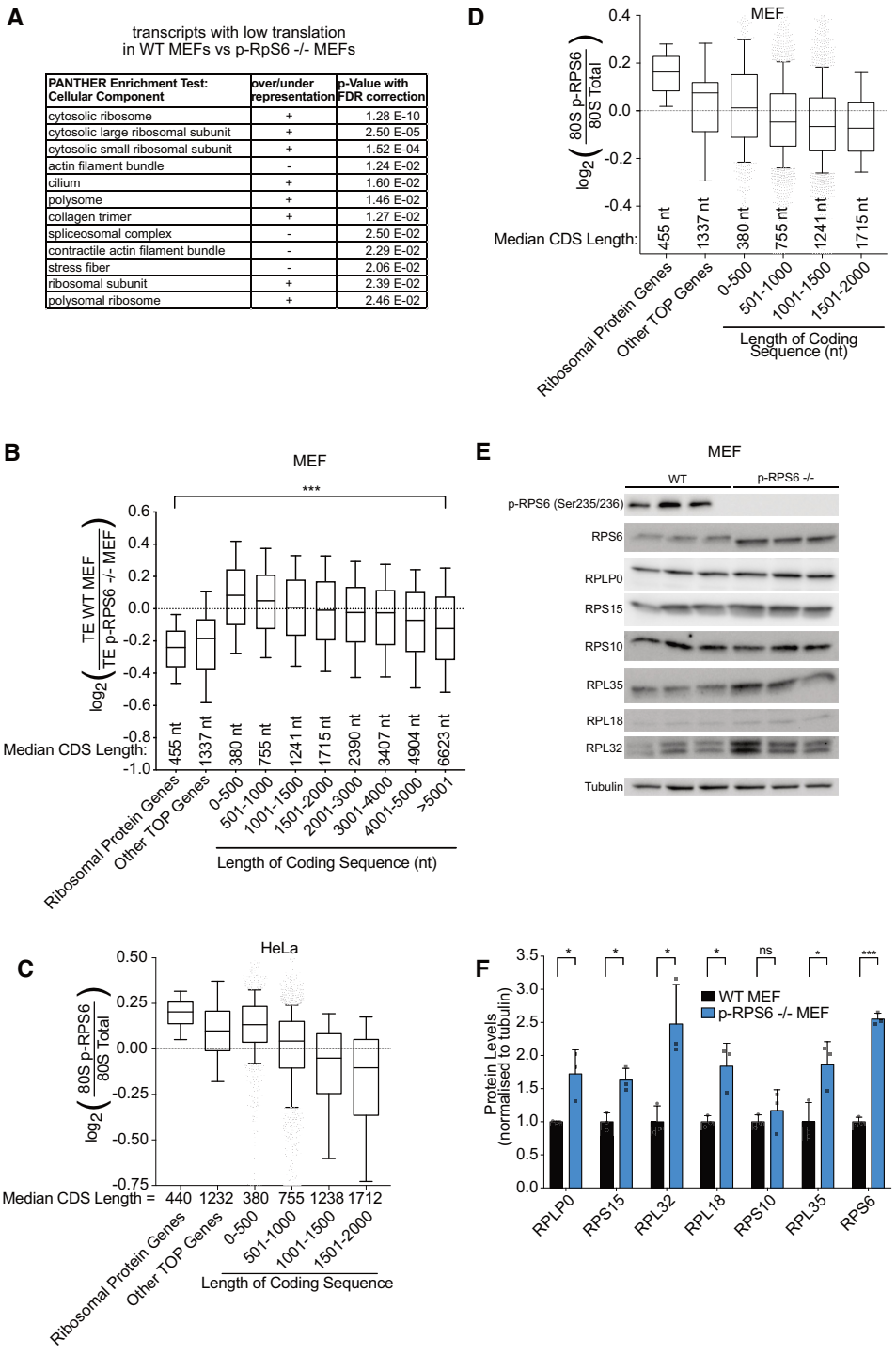

Figure 5. TOP mRNAs are efficiently translated independently of RPS6 phosphorylation. (**A**) mRNAs encoding ribosomal proteins are enriched among the set of transcripts with low translation efficiency in control MEFs compared to rpS6$^{P-/-}$ MEFs. For each transcript the ratio of (translation efficiency in control MEFs)/(translation efficiency in rpS6$^{P-/-}$ MEFs) was calculated and GO enrichment analysis for cellular component was then computed using PANTHER. (**B**) Ribosomal protein and TOP-containing mRNAs are not induced in the presence of pRPS6. Grouped analysis of translational efficiency in mouse embryonic fibroblasts. Genes were classified into the indicated groups. Line = median, boxes = upper and lower quartile boundaries, whiskers = first and last decile boundaries. *P*-values were determined using unpaired, two-sided Kruksal Wallis tests, *P*-values were adjusted for multiple testing using statistical hypothesis testing, $***P < 0.0002$. (C, D) Ribosomal protein and TOP-containing mRNAs are translated by ribosomes phosphorylated on RPS6 in both HeLa (**C**) and MEF cells (**D**). Grouped analysis of p-RPS6 occupancy for transcripts grouped as indicated. Line = median, boxes = upper and lower quartile boundaries, whiskers = first and last decile boundaries. (E, F) rpS6$^{P-/-}$ MEF cells have elevated levels of ribosomal proteins. (**E**) Western blot analysis of ribosomal proteins in wildtype control and rpS6$^{P-/-}$ MEF cells. Three biological replicates for each genotype are shown. Equal amounts of total protein were loaded per lane. Tubulin was used as a loading control. (**F**) Quantification of protein band intensity normalized to tubulin. *P*-values were calculated using unpaired, two-sided *t*-tests. $*P < 0.05$, $***P < 0.0005$.

are not equally depleted across the entire length of the transcript. Instead, they are present at higher levels at the 5′ end of the ORF and then decrease, as can be seen for instance on the POLR2A mRNA (Figure 2A). This trend can be seen transcriptome-wide, for instance on a metagene plot of all ORFs longer than 3000nt (Figure 2B). Since this decrease occurs slowly and progressively with distance from the translation start codon, it is not visible on short ORFs (Figure 2C), and it causes longer ORFs to have a lower average pS6 abundance when integrated over the entire transcript length. Consequently, transcriptome-wide, the longer the ORF, the lower the average pS6 abundance (Figure 2D). We confirmed this result by immunoprecipitating ribosomes containing pS6 and quantifying the enrichment of bound mRNAs by Q-RT-PCR, showing that indeed mRNAs with long CDSs are less enriched compared to mRNAs with short CDSs (Figure 2E). Since we are calculating the ratio of pS6-ribosomes to total ribosomes, this implies that the abundance of non-phosphorylated ribosomes progressively increases on long ORFs. In sum, ribosomes are most highly phosphorylated on RPS6 at the 5′end of CDSs, and gradually become dephosphorylated as they elongate. A previous report showed that S6K, the kinase responsible for phosphorylating RPS6, is physically associated to preinitiation complexes, which are 40S ribosomes bound to translation initiation factors (eIFs), and that this association occurs via eIF3 (24). We previously showed that in human cells ribosomes remain bound to eIFs while they scan the 5′UTR of mRNAs up to the main ORF start codon, and then progressively release the eIFs, including eIF3, over the first few rounds of elongation (20). Hence a model consistent with all these data is that 40S subunits become phosphorylated on RPS6 by S6K during 5′UTR scanning (Figure 2F). Once the 40S converts to an 80S ribosome and undergoes several rounds of peptide elongation, eIF3 and S6K are released, allowing S6 to become progressively dephosphorylated as the ribosome elongates.

Dephosphorylation rate of RPS6 depends on mRNA environment

Although there is a general trend of lower RPS6 phosphorylation on mRNAs with longer CDS, nonetheless a scatter plot of phospho-RPS6 abundance versus CDS length shows quite a lot of dispersion (Supplementary Figure S2A), indicating that other factors also influence RPS6 abundance. To find such other factors, we did two analyses: First, we ranked all mRNAs according to their relative abundance of phospho-RPS6 reads and performed a gene set enrichment analysis using PANTHER (25). mRNAs coding for plasma membrane proteins, which are translated on the endoplasmic reticulum (ER), were enriched for low phospho-RPS6, whereas mRNA encoding for nuclear or cytosolic proteins were enriched for high phospho-RPS6 (Figure 3A, Supplementary Table S6). Secondly, we did a GO enrichment analysis on the set of mRNAs with lowest phospho-RPS6 abundance and conversely found an enrichment for ER-translated mRNAs and a de-enrichment for mRNAs encoding nuclear and cytosolic components (Figure 3B, Supplementary Table S7). We therefore selected all mRNAs that are translated on the ER, encoding secreted proteins, plasma-membrane integral proteins and ER/Golgi proteins based on (26) (see Materials & Methods) and found that indeed for almost all CDS length categories these mRNAs have lower phospho-RPS6 counts than average (Figure 3C, D). A position-resolved metagene plot of phospho-RPS6 abundance for ER-translated mRNAs versus all other mRNAs (Figure 3E) revealed that ribosomes translating on the ER are less phosphorylated from nt 120 on the CDS (once the nascent signal peptide has emerged from the ribosome exit tunnel and is recognized by the Signal Recognition Particle (SRP)) to nt 400 on the CDS. After that, they are dephosphorylated with the same rate as all other mRNAs. This discrete phase of increased dephosphorylation may be due to translational slowdown or pausing during SRP-recognition (27,28), or to some other effect of the SRP on the ribosome. For instance, analysis of eIF3B-selective 80S ribosome footprints (20) shows that SRP-binding also correlates with an earlier disengagement of initiation factors from the elongating ribosome (Supplementary Figure S2B). In contrast, ribosomes translating mRNAs encoding nuclear proteins (GO:0031981) are more phosphorylated than average, although the magnitude of this effect is small (Figures 3F-G). Correspondingly, ribosomes translating mRNAs with long CDSs that encode for nuclear proteins tend to be more resistant to dephosphorylation as they move down the CDS, with pS6-footprint density not dropping as much compared to total 80S footprints (cf. Supplementary Figure S2C to Figure 2A). Together, these data suggest that the rate of dephosphorylation of RPS6 might depend on the subcellular environment in which the ribosomes reside.

Transcripts with short CDSs are translated less efficiently in rpS6$^{P-/-}$ cells

From the results shown above, we hypothesized that RPS6 phosphorylation differentially affects translation of mRNAs depending on their CDS length. To test this functionally, we performed pS6-selective and standard ribosome footprinting in wildtype and rpS6$^{P-/-}$ mouse embryonic fibroblasts (MEFs), where the phosphorylated serines (235, 236, 240, 244 and 247) on endogenous rpS6 were mutated to alanine (16) (Supplementary Figure S3A). As with HeLa cells, the p-RPS6 immunoprecipitation was highly specific in MEFs, co-precipitating ribosomes (RPS15) only from wildtype but not rpS6$^{P-/-}$ cells (Supplementary Figure S3B). Indeed, the RNA yield of p-RPS6 IPs from rpS6$^{P-/-}$ MEFs was so low that we could not generate a footprint library to sequence it, highlighting the specificity of the IPed material in control MEFs. As in HeLa cells, ribosome footprinting in MEFs yielded the expected triplet periodicity and enrichment in CDSs of translating 80S ribosomes (Supplementary Figure S3C, D). As expected, the mRNAs with lowest pS6-abundance transcriptome-wide were mitochondrially encoded mRNAs (Supplementary Figure S3E). (We did not detect mitochondrial mRNAs in our HeLa footprinting experiments.) As in human cells, mRNAs translated on the ER were enriched among the transcripts with low pS6 abundance, whereas cytosolically-translated mRNAs were de-enriched (Supplementary Table S8). Likewise, we observed reduced levels of pS6 on long transcripts in

MEFs, although the effect was weaker than in HeLa cells (Figure 4A, Supplementary Figure S3F). Nonetheless, the progressive loss of RPS6 phosphorylation is clearly visible on single transcripts with long CDSs such as EP400 (Figure 4B) and on a metagene plot for all transcripts with long CDS >3000 nt (red trace, Figure 4D), indicating it is a conserved feature of translation in humans and mice. Interestingly, when comparing the translation efficiency for each transcript in wildtype MEFs to rpS6$^{P-/-}$ mutant MEFs, we found that RPS6 phosphorylation affects translation in a CDS-length dependent manner. The presence of RPS6 phosphorylation in wildtype MEFs increases translation of mRNA with short CDSs but not of mRNAs with long CDSs (Figure 4C). This effect is mostly driven by changes in the number of ribosome footprints per transcript (Supplementary Figure S3G) and not by changes in mRNA levels (Supplementary Figure S3H), indicating that a translational mechanism is at play. Hence RPS6 phosphorylation increases translation of mRNAs with short CDSs, which are the ones with the highest levels of pS6-ribosomes on them.

Since RPS6 becomes progressively dephosphorylated on long CDSs as ribosomes move down the CDS, we asked whether we could observe position-dependent effects on translation in the rpS6$^{P-/-}$ MEFs. We expected that loss of RPS6 phosphorylation at the 5′end of the CDSs, where RPS6 phosphorylation is normally high, could lead to a change in ribosome density, whereas at the 3′end where RPS6 levels are low in wildtype MEFs, loss of S6 phosphorylation would have no effect. This, however, was not the case; Ribosome footprint density was similar along the entire length of long CDSs in WT and rpS6$^{P-/-}$ MEFs (Figure 4D). Therefore, position-dependent differences in pS6 abundance do not lead directly to position-dependent changes in ribosome density, suggesting that pS6 does not affect translation speed.

Interestingly, in wildtype MEFs, in rpS6$^{P-/-}$ MEFs, and in HeLa cells total 80S ribosome density decreases with distance from the 5′end of the CDSs (black curves in Figures 2D and 4D). This suggests either that a significant fraction of ribosomes abort protein synthesis prematurely or that ribosomes progressively speed up (analogous to cars speeding up after a traffic jam, leading to lower car density). Irrespective of which explanation is correct, however, this occurs to the same extent in both WT and rpS6$^{P-/-}$ MEFs (Figure 4D). Hence, neither premature translation termination, nor elongation speed appear to be affected by RPS6 phosphorylation. Furthermore, in WT MEFs compared to rpS6$^{P-/-}$MEFs, transcripts with short CDSs had uniformly elevated ribosome density throughout the entire length of the CDS, from the start codon onwards (Figure 4E). One possible explanation is that, through an unknown mechanism which will require further investigation, the phosphorylation of RPS6 on ribosomes when they terminate translation of short CDSs increases translation initiation rates on those transcripts.

Translation of 5′ TOP mRNAs is resistant to loss of RpS6 phosphorylation

We noticed that one set of transcripts appears to defy the global trends described above. As discussed above, RPS6 phosphorylation increases most the translation of mRNAs with short CDSs (Figure 4C). We asked what transcripts are present in the opposite category—the ones that do not increase in translation efficiency in the presence of RPS6 phosphorylation. In addition to the expected transcripts with long CDSs (Figure 4C) we also found mRNAs containing 5′ terminal oligopyrimidine tract (TOP) motifs: A Gene Ontology (GO) enrichment analysis on the set of transcripts with a low ratio of translation efficiency in wildtype MEFs versus rpS6$^{P-/-}$ MEFs found transcripts coding for ribosomal proteins to be most highly enriched (Figure 5A). Indeed, when comparing wildtype to rpS6$^{P-/-}$ MEFs, translation of mRNAs encoding ribosomal proteins does not increase (Figure 5B, Supplementary Figure S4A), which is surprising because ribosomal proteins are short (median CDS length of 455 nt) and therefore would be expected to increase in translation efficiency in the presence of RPS6 phosphorylation, like other short ORF mRNAs. Transcripts encoding ribosomal proteins contain 5′ TOP motifs (29). We found that other TOP mRNAs that do not code for ribosomal proteins also did not benefit in terms of translation efficiency in wildtype MEFs compared to rpS6$^{P-/-}$ MEFs considering their CDS length (Figure 5B, Supplementary Figure S4A). One explanation could be that, despite their short length, TOP mRNAs are preferentially translated by ribosomes lacking RpS6 phosphorylation. This, however, was not the case: In both HeLa and MEFs, ribosomal and TOP mRNAs have high levels of p-RPS6-ribosome footprints (Figure 5C, D, Supplementary Figure S4B–D). Seen from the opposite perspective, translation of TOP-motif-containing mRNAs does not decrease when RPS6 phosphorylation decreases, suggesting they may be translated using a different mechanism that bypasses the effect for RpS6 phosphorylation. It is tempting to speculate this may be due to a role of LARP1 (29), but future work will be required to test this. In agreement with these footprinting data, rpS6$^{P-/-}$ MEFs have elevated levels of ribosomal proteins compared to control MEFs (Figure 5E-F). This is not due to a general increase in mTOR signaling as a compensation to p-RPS6 mutation since mTOR target phosphorylation is unchanged in rpS6$^{P-/-}$ MEFs (Supplementary Figure S4E). Increased levels of ribosomes may explain the global increase in protein synthesis rates previously observed in rpS6$^{P-/-}$ MEFs (16).

DISCUSSION

We previously developed a method for selective 40S and 80S ribosome profiling in human cells which employs an immunoprecipitation strategy to identify the location on endogenous mRNAs of ribosomes bound to a factor of interest, such as an initiation factor (20). Here, we extend that method to look at ribosomes containing a post-translational modification of interest, in this case phosphorylation of RPS6. This modification-selective ribosome footprinting is a method that can be used in the future to study also other ribosome modifications, such as ribosome ubiquitination upon UPR activation (7), ribosome N(α)-acetylation which promotes ribosome activity (12) as well as modifications of ribosome interacting proteins such as translation initiation factors (30–32).

We find that RPS6 phosphorylation is highest on ribosomes positioned on the start codons of main Open Reading Frames (ORF), and then progressively decreases as ribosomes translate the ORF, making this drop most relevant on mRNAs with long ORFs. It was previously shown that S6K, the kinase that phosphorylates RPS6, is physically associated to pre-initiation complexes—scanning 40S ribosomes that are bound to initiation factors—via eIF3 (24). We previously showed that ribosomes are bound to eIF3 during the entirety of the scanning process and during the first few rounds of peptide elongation, after which they let go of eIF3 (20). Hence, one likely molecular model that could explain these observations is that RPS6 becomes phosphorylated by S6K while it is part of a scanning 40S ribosome that is associated to eIF3 and hence S6K. After the first few rounds of peptide elongation, the 80S ribosome lets go of eIF3, and hence S6K, thereby allowing for the phosphatase-mediated progressive dephosphorylation of RPS6 (Figure 2D). It is possible that the dephosphorylation of RpS6 along a CDS depends on (i) the time elapsed since the translating ribosome released the eIFs and S6K, or (ii) the distance separating the translating ribosome from the cap/5′UTR, which contains other scanning ribosomes with eIFs and S6K. Future work will be required to distinguish these two possibilities.

The data we provide here indicate that RPS6 phosphorylation has a functional consequence on translation. In wildtype cells containing RPS6 phosphorylation, compared to $rpS6^{P-/-}$ mutant MEFs lacking RPS6 phosphorylation, we observe elevated translation efficiency of mRNAs with short CDSs, which are the ones with high RPS6 phosphorylation (Supplementary Figure S5A). In contrast, mRNAs with longer CDSs, and hence lower RPS6 phosphorylation, do not show an increase in translation efficiency. Mysteriously, the state of RPS6 phosphorylation of ribosomes as they reach the end of a CDS seems to affect translation efficiency on the entirety of that mRNA. One possible explanation is that initiation rates on an mRNA are increased if ribosomes terminating translation on that mRNA are still phosphorylated on RPS6. We do not know how this 3′-to-5′ information flow works mechanistically, however previous studies suggest such a flow exists (33). This could occur if mRNAs are circularized via interactions between the poly-A tail and the 5′cap and RPS6 phosphorylation promotes ribosome re-loading for a new round of translation. On longer ORFs, ribosomes would be preferentially dephosphorylated when they terminate, reducing initiation rates. Alternatively, RPS6 could affect circularization itself. A hint to the relevant mechanism comes from the fact that mRNAs containing 5′ TOP motifs seem to evade this regulatory mechanism. Further work will be necessary to unravel these mechanisms.

Interestingly, we noticed that on average, on mRNAs with long CDSs, ribosome density decreases towards the 3′ end of the CDS. This happens in all cell lines we studied - both in human cells (Figure 2B) and in mouse cells (Figure 4D), and in both $RpS6^{WT}$ and $RpS6^{-/-}$ cells (Figure 4D). Hence, this phenomenon has nothing to do with RpS6 phosphorylation. Nonetheless, we believe this is an interesting observation and provide here some hypotheses for future study as to why this is occurring. One possible interpretation is that a significant fraction of ribosomes abort protein synthesis prematurely and drop off. Although ribosome drop-off does occur (34), it would need to happen ∼30% of the time to account for the magnitude of the drop we observe here in mammalian cells (Figures 2B and 4D). This would lead to 30% of large proteins being synthesized as truncated proteins. Alternatively, this indicates that ribosomes progressively increase their translation speed towards the 3′ end of the CDS. This could potentially prevent ribosome collisions, which would occur if ribosomes translate with a uniform speed. As ribosomes translate, stochastic events cumulatively influence the distance separating two ribosomes, such that a distance that is sufficient to prevent collisions early at the 5′ end of an ORF may become insufficient after many rounds of elongation (Supplementary Figure S5B). A progressive acceleration in translation speed could counteract this effect.

In sum, we find here that the phosphorylation of ribosomes on RPS6 depends on their position on an mRNA, and show that RPS6 phosphorylation has an effect on mRNA translation. The method of selective footprinting that we use here can be used in the future to study other post-translational modifications of the ribosome.

DATA AVAILABILITY

All deep sequencing datasets have been submitted to NCBI Geo (GSE168977). Custom software is available on GitHub: https://github.com/aurelioteleman/Teleman-Lab.

SUPPLEMENTARY DATA

Supplementary Data are available at NAR Online.

ACKNOWLEDGEMENTS

We thank Oded Meyuhas for kindly providing the p-S6 mutant MEF cells and Ramona Weber for scientific discussion. *Author contributions:* M.R. performed the experiment in Figure 2E. J.B. performed all other experiments. J.B., M.R. and A.T. designed the work, analyzed data, interpreted data and wrote the manuscript.

FUNDING

DKFZ NCT3.0 Integrative Project in Cancer Research grant [NCT3.0_2015.54 DysregPT to A.A.T]. Funding for open access charge: Core budget.
Conflict of interest statement. None declared.

REFERENCES

1. Simsek,D. and Barna,M. (2017) An emerging role for the ribosome as a nexus for post-translational modifications. *Curr. Opin. Cell Biol.*, **45**, 92–101.
2. Henras,A.K., Soudet,J., Gerus,M., Lebaron,S., Caizergues-Ferrer,M., Mougin,A. and Henry,Y. (2008) The post-transcriptional steps of eukaryotic ribosome biogenesis. *Cell. Mol. Life Sci.*, **65**, 2334–2359.
3. Penzo,M. and Montanaro,L. (2018) Turning uridines around: role of rRNA pseudouridylation in ribosome biogenesis and ribosomal function. *Biomolecules*, **8**, 38.

4. Granneman,S. and Baserga,S.J. (2004) Ribosome biogenesis: of knobs and RNA processing. *Exp. Cell Res.*, **296**, 43–50.
5. Mazumder,B., Sampath,P., Seshadri,V., Maitra,R.K., DiCorleto,P.E. and Fox,P.L. (2003) Regulated release of L13a from the 60S ribosomal subunit as a mechanism of transcript-specific translational control. *Cell*, **115**, 187–198.
6. Gressner,A.M. and Wool,I.G. (1974) The phosphorylation of liver ribosomal proteins in vivo. Evidence that only a single small subunit protein (S6) is phosphorylated. *J. Biol. Chem.*, **249**, 6917–6925.
7. Higgins,R., Gendron,J.M., Rising,L., Mak,R., Webb,K., Kaiser,S.E., Zuzow,N., Riviere,P., Yang,B., Fenech,E. *et al.* (2015) The Unfolded Protein Response Triggers Site-Specific Regulatory Ubiquitylation of 40S Ribosomal Proteins. *Mol. Cell*, **59**, 35–49.
8. Silva,G.M., Finley,D. and Vogel,C. (2015) K63 polyubiquitination is a new modulator of the oxidative stress response. *Nat. Struct. Mol. Biol.*, **22**, 116–123.
9. Xirodimas,D.P., Sundqvist,A., Nakamura,A., Shen,L., Botting,C. and Hay,R.T. (2008) Ribosomal proteins are targets for the NEDD8 pathway. *EMBO Rep.*, **9**, 280–286.
10. Couttas,T.A., Raftery,M.J., Padula,M.P., Herbert,B.R. and Wilkins,M.R. (2012) Methylation of translation-associated proteins in *Saccharomyces cerevisiae*: identification of methylated lysines and their methyltransferases. *Proteomics*, **12**, 960–972.
11. Walczak,C.P., Leto,D.E., Zhang,L., Riepe,C., Muller,R.Y., DaRosa,P.A., Ingolia,N.T., Elias,J.E. and Kopito,R.R. (2019) Ribosomal protein RPL26 is the principal target of UFMylation. *PNAS*, **116**, 1299–1308.
12. Kamita,M., Kimura,Y., Ino,Y., Kamp,R.M., Polevoda,B., Sherman,F. and Hirano,H. (2011) N(alpha)-Acetylation of yeast ribosomal proteins and its effect on protein synthesis. *J. Proteomics*, **74**, 431–441.
13. Biever,A., Valjent,E. and Puighermanal,E. (2015) Ribosomal protein S6 phosphorylation in the nervous system: from regulation to function. *Front. Mol. Neurosci.*, **8**, 75.
14. Meyuhas,O. (2015) Ribosomal protein S6 phosphorylation: four decades of research. *Int. Rev. Cell Mol. Biol.*, **320**, 41–73.
15. Yerlikaya,S., Meusburger,M., Kumari,R., Huber,A., Anrather,D., Costanzo,M., Boone,C., Ammerer,G., Baranov,P.V. and Loewith,R. (2016) TORC1 and TORC2 work together to regulate ribosomal protein S6 phosphorylation in *Saccharomyces cerevisiae*. *Mol. Biol. Cell*, **27**, 397–409.
16. Ruvinsky,I., Sharon,N., Lerer,T., Cohen,H., Stolovich-Rain,M., Nir,T., Dor,Y., Zisman,P. and Meyuhas,O. (2005) Ribosomal protein S6 phosphorylation is a determinant of cell size and glucose homeostasis. *Genes Dev.*, **19**, 2199–2211.
17. Ruvinsky,I., Katz,M., Dreazen,A., Gielchinsky,Y., Saada,A., Freedman,N., Mishani,E., Zimmerman,G., Kasir,J. and Meyuhas,O. (2009) Mice deficient in ribosomal protein S6 phosphorylation suffer from muscle weakness that reflects a growth defect and energy deficit. *PLoS One*, **4**, e5618.
18. Xu,J., Chen,J., Dong,Z., Meyuhas,O. and Chen,J.K. (2015) Phosphorylation of ribosomal protein S6 mediates compensatory renal hypertrophy. *Kidney Int.*, **87**, 543–556.
19. Granot,Z., Swisa,A., Magenheim,J., Stolovich-Rain,M., Fujimoto,W., Manduchi,E., Miki,T., Lennerz,J.K., Stoeckert,C.J. Jr, Meyuhas,O *et al.* (2009) LKB1 regulates pancreatic beta cell size, polarity, and function. *Cell Metab.*, **10**, 296–308.
20. Bohlen,J., Fenzl,K., Kramer,G., Bukau,B. and Teleman,A.A. (2020) Selective 40S footprinting reveals cap-tethered ribosome scanning in human cells. *Mol. Cell*, **79**, 561–574.
21. Schibich,D., Gloge,F., Pohner,I., Bjorkholm,P., Wade,R.C., von Heijne,G., Bukau,B. and Kramer,G. (2016) Global profiling of SRP interaction with nascent polypeptides. *Nature*, **536**, 219–223.
22. Wagner,S., Herrmannova,A., Hronova,V., Gunisova,S., Sen,N.D., Hannan,R.D., Hinnebusch,A.G., Shirokikh,N.E., Preiss,T. and Valasek,L.S. (2020) Selective translation complex profiling reveals staged initiation and co-translational assembly of initiation factor complexes. *Mol. Cell*, **79**, 546–560.
23. Oh,E., Becker,A.H., Sandikci,A., Huber,D., Chaba,R., Gloge,F., Nichols,R.J., Typas,A., Gross,C.A., Kramer,G. *et al.* (2011) Selective ribosome profiling reveals the cotranslational chaperone action of trigger factor in vivo. *Cell*, **147**, 1295–1308.
24. Holz,M.K., Ballif,B.A., Gygi,S.P. and Blenis,J. (2005) mTOR and S6K1 mediate assembly of the translation preinitiation complex through dynamic protein interchange and ordered phosphorylation events. *Cell*, **123**, 569–580.
25. Mi,H., Ebert,D., Muruganujan,A., Mills,C., Albou,L.P., Mushayamaha,T. and Thomas,P.D. (2021) PANTHER version 16: a revised family classification, tree-based classification tool, enhancer regions and extensive API. *Nucleic Acids Res.*, **49**, D394–D403.
26. Jan,C.H., Williams,C.C. and Weissman,J.S. (2014) Principles of ER cotranslational translocation revealed by proximity-specific ribosome profiling. *Science*, **346**, 1257521.
27. Pechmann,S., Chartron,J.W. and Frydman,J. (2014) Local slowdown of translation by nonoptimal codons promotes nascent-chain recognition by SRP in vivo. *Nat. Struct. Mol. Biol.*, **21**, 1100–1105.
28. Lakkaraju,A.K., Mary,C., Scherrer,A., Johnson,A.E. and Strub,K. (2008) SRP keeps polypeptides translocation-competent by slowing translation to match limiting ER-targeting sites. *Cell*, **133**, 440–451.
29. Cockman,E., Anderson,P. and Ivanov,P. (2020) TOP mRNPs: molecular mechanisms and principles of regulation. *Biomolecules*, **10**, 969.
30. Proud,C.G. (2015) Mnks, eIF4E phosphorylation and cancer. *Biochim. Biophys. Acta*, **1849**, 766–773.
31. Morley,S.J., Coldwell,M.J. and Clemens,M.J. (2005) Initiation factor modifications in the preapoptotic phase. *Cell Death Differ.*, **12**, 571–584.
32. Duncan,R. and Hershey,J.W. (1984) Heat shock-induced translational alterations in HeLa cells. Initiation factor modifications and the inhibition of translation. *J. Biol. Chem.*, **259**, 11882–11889.
33. Fernandes,L.D., Moura,A.P.S. and Ciandrini,L. (2017) Gene length as a regulator for ribosome recruitment and protein synthesis: theoretical insights. *Sci. Rep.*, **7**, 17409.
34. Sin,C., Chiarugi,D. and Valleriani,A. (2016) Quantitative assessment of ribosome drop-off in E. coli. *Nucleic Acids Res.*, **44**, 2528–2537.
35. Langmead,B. and Salzberg,S.L. (2012) Fast gapped-read alignment with Bowtie 2. *Nat. Methods*, **9**, 357–359.